JTTEE5 16:669–676
DOI: 10.1007/s11666-007-9089-5
1059-9630/$19.00 © ASM International 2007

Peer Reviewed

# Microstructural Characterization of Cold-Sprayed Nanostructured FeAl Intermetallic Compound Coating and its Ball-Milled Feedstock Powders

*Hong-Tao Wang, Chang-Jiu Li, Guan-Jun Yang, Cheng-Xin Li, Qiang Zhang, and Wen-Ya Li*

*(Submitted March 9, 2007; in revised form June 21, 2007)*

**It is difficult to deposit dense intermetallic compound coatings by cold spraying directly using the compound feedstock powders due to their intrinsic low-temperature brittleness. A method to prepare intermetallic compound coatings in-situ employing cold spraying was developed using a metastable alloy powder assisted with post-heat treatment. In this study, a nanostructured Fe/Al alloy powder was prepared by ball-milling process. The cold-sprayed Fe/Al alloy coating was evolved in-situ to intermetallic compound coating through a post-heat treatment. The microstructural evolution of the Fe-40Al powder during mechanical alloying and the effect of the post-heat treatment on the microstructure of the cold-sprayed Fe(Al) coating were characterized by optical microscopy, scanning electron microscopy, transmission electron microscopy (TEM), and x-ray diffraction analysis. The results showed that the milled Fe-40Al powder exhibits lamellar microstructure. The microstructure of the as-sprayed Fe(Al) coating depends significantly on that of the as-milled powder. The heat-treatment temperature significantly influences the in-situ evolution of the intermetallic compound. The heat treatment at a temperature of 500 °C results in the complete transformation of Fe(Al) solid solution to FeAl intermetallic compound.**

**Keywords** ball milling, cold spray, FeAl, heat treatment, microstructure, nanocrystalline material

## 1. Introduction

Recently, cold spraying as a new emerging coating process has been widely investigated owing to capability to deposit many highly pure metallic or composite coatings (Ref 1-4). In this process, spray particles are accelerated by a low-temperature supersonic gas flow to a high velocity (300-1,200 m/s). The deposition of particles takes place through intensive plastic deformation upon impact in a solid state at a temperature well below the melting point of spray materials. Consequently, the deleterious effects inherent to conventional thermal spraying such as oxidation, phase transformation, decomposition, grain growth, and other problems can be minimized or eliminated (Ref 1). This low-temperature characteristic of cold spraying makes it potential to deposit the coating of temperature sensitive materials such as nanostructured powder (Ref 5-8).

Mechanical alloying is one of the most common methods to develop nanocrystalline alloying powder due to its simplicity, the relatively inexpensive equipment, and the applicability to essentially all kinds of materials (Ref 9). Therefore, the combination of cold spraying and mechanical alloying process provides the opportunity to produce a complete nanostructured coating. Recently, some nanostructured coatings, such as metallic aluminum (Ref 8), Ni (Ref 10), and Fe-Si (Ref 7) alloys have been deposited by cold spraying of the milled powder.

Iron aluminides intermetallic alloys are attractive materials for several industrial applications from medium to high temperatures (Ref 11-13), either as bulk materials or as coatings owing to their good mechanical properties, relatively low density (5.56 g/cm$^3$), low cost, and excellent corrosion resistance in oxidizing and sulfidizing atmospheres which is relied on their ability to form a highly protective $Al_2O_3$ scale (Ref 14, 15). Compared to steels and other commercial Fe-based alloy, FeAl alloy exhibits improved oxidation resistance and lower density. In addition, FeAl also has a high-electrical resistivity (130-170 μΩ/cm). However, industrial application of these alloys has been limited due to their poor ductility and fracture toughness at room temperature (Ref 14). There

This article is an invited paper selected from presentations at the 2007 International Thermal Spray Conference and has been expanded from the original presentation. It is simultaneously published in *Global Coating Solutions, Proceedings of the 2007 International Thermal Spray Conference*, Beijing, China, May 14-16, 2007, Basil R. Marple, Margaret M. Hyland, Yuk-Chiu Lau, Chang-Jiu Li, Rogerio S. Lima, and Ghislain Montavon, Ed., ASM International, Materials Park, OH, 2007.

**Hong-Tao Wang, Chang-Jiu Li, Guan-Jun Yang, Cheng-Xin Li, Qiang Zhang,** and **Wen-Ya Li**, State Key Laboratory for Mechanical Behavior of Materials, School of Materials Science and Engineering, Xi'an Jiaotong University, Xi'anShaanxi, 710049, P.R. China. Contact e-mail: licj@mail.xjtu.edu.cn.

are several possible ways to improve these two major drawbacks, such as grain boundary strength (Ref 16, 17), oxidation dispersion strength (Ref 18), and grain refinement (Ref 19-24). The synthesis and development of FeAl intermetallic compound materials with nanocrystalline structures have been attracting increasing interests in the last decades not only due to the enhanced hardness and strength found, but also because of expectations of improved ductility and toughness comparing with their coarse-grained counterparts (Ref 19, 22).

Thermal spray processes (e.g., high velocity oxygen-fuel (HVOF) spray and plasma spray) have been used to deposit nanostructured intermetallic coatings using milled intermetallic compound powders (Ref 25-27). However, the oxidation that occurs during spraying changes the composition and microstructure design of the powders and deteriorates the properties of the deposits. Cold spraying is promising to deposit coatings without composition change. However, cold spraying coating is generally deposited through plastic deformation of sprayed particles. Due to the intrinsic brittleness of intermetallic compounds at low temperatures, it is difficult to deposit intermetallic coatings using directly the intermetallic compound powder feedstock.

Our previous study showed that the nanostructured FeAl/WC intermetallic compound based composite coating can be produced by cold spraying milled powders assisted by a post-heat treatment (Ref 28). It was found that the nanostructure of the as-milled powder was retained in the coating. Moreover, the microstructure of the as-milled powder exhibits a significant effect on the microstructure of the cold-sprayed coating. In the present paper, a nanostructured FeAl intermetallic compound coating was produced by post-heat treatment of cold-spayed Fe(Al) solid solution precursor deposit. The microstructure evolution of powder during ball milling was investigated. The correlation between microstructure of milled powder and corresponding cold-sprayed coating was examined. Moreover, the effect of the post-heat treatment on the phase evolution and microstructure of the coating was also investigated.

## 2. Experimental Materials and Procedures

### 2.1 Feedstock Powder Preparation

The commercially available Fe (99.8 wt.%, −54 μm, Youxinglian Nonferrous Metals Ltd, Beijing, China) and Al (99.5 wt.%, −74 μm, Youxinglian Nonferrous Metals Ltd, Beijing, China) powders were used as starting materials to produce a composite feedstock powder with a composition corresponding to $Fe_{60}Al_{40}$. The oxygen contents of the initial Fe and Al powders determined using an oxygen determinator (RO-316, LECO, USA) were 0.52 wt.% and 0.8 wt.%, respectively. The powder mixtures were loaded into a 250 mL stainless steel vial together with two different sizes of the stainless steel balls (10 and 5 mm in diameter). The vial was filled with argon during milling. Ball milling was performed in a high-energy ball mill with a ball-to-powder weight ratio of 10:1 at a rotation speed of 180 rpm for various durations. Powder samples were taken from the mill at selected time intervals for analysis. The powder milled for 36 h was sieved to a size less than 45 μm and chosen as the feedstock powder for spraying deposition.

### 2.2 Coating Preparation and Heat Treatment

The home-made cold spraying system was employed to deposit the coatings in this study. A spray gun with a converging-diverging de Laval type nozzle of a throat diameter of 2 mm was adopted. The detailed information about this system has been depicted elsewhere (Ref 4). Nitrogen gas was employed as both accelerating and powder feeding gases used at a pressure of 2.0 and 2.5 MPa, respectively, and a temperature of 510 °C in the pre-chamber. The standoff distance from the nozzle exit to substrate surface was 15 mm. During deposition, the spray gun was manipulated by a robot at a traverse speed of 40 mm/s relative to the substrate. Stainless steel was used as a substrate. Its surface was sandblasted using 24 mesh alumina grits before coating deposition. The coating was deposited by six passes of spraying and the mean thickness per pass was about 35 μm. The as-sprayed coating was then annealed at different temperatures in a furnace in argon atmosphere.

### 2.3 Powder and Coating Characterization

The cross-sectional microstructure of the powder and coatings were characterized using optical microscopy (OM) (MeF3A, REICHERT-JUNG, Austria), scanning electron microscopy (SEM) (JSM-5800, JEOL, Tokyo, Japan), field-emission scanning electron microscopy (FE-SEM) (JSM-6700F, JEOL, Tokyo, Japan) equipped with energy disperse x-ray analysis (EDXA). The crystalline structure evolution of the powder during the ball milling and the coating during heat treatment was characterized by x-ray diffraction diffractometer (XRD) (XRD-6000, Shimadzu, Kyoto, Japan) using Cu $K\alpha$ radiation. The size distribution of the milled powder was determined by a laser diffraction sizer (MASTERSIZER 2000, Malvern Instruments Ltd, UK). The oxygen contents of the milled powders and corresponding coating were determined using an oxygen determinator (RO-316, LECO, USA). Chemical analysis of the as-milled powder and coating before and after heat treatment was performed using inductively coupled plasma-optical emission spectrometer (ICP) (IRISIntrepid II XSP, PE, USA) and all analyses were conducted in triplicate.

The grain size of the as-milled powders and the coatings was estimated using the Scherrer formula by taking into account of Cu $K\alpha_1$ radiation, after $K\alpha_2$ stripping using the Rachinger method. The XRD peak broadening was attributed to instrumental factor and physical factors such as crystallite size and lattice strains (Ref 29). To correct for the instrumental factor, the same Fe powder but annealed at 1,073 K for 24 h to eliminate any effects of grain size and internal strain was used as standard powder and

assuming a Gaussian peak shape for both the instrumental and the sample peak functions. Thus, the ''pure'' breadth at half maximum intensity of the sample peak can be obtained by excluding instrumental broadening. Then, the average grain size was estimated using the Scherrer formula according to the discussion by Shaw et al. (Ref 30).

Analyses of the grain size and crystal structure of the coating were also performed using transmission electron microscopy (TEM) (JEM-200CX, JEOL, Tokyo, Japan). To investigate the coatings by TEM, discs of 3 mm diameter were punched from sheets of the coatings, and then polished, dimpled, and ion milled in a dual ion mill (Model 691, GATAN Co, USA).

## 3. Results and Discussion

### 3.1 Characterization of the Milled Powder

Figure 1 shows XRD patterns of the starting Fe-Al powder mixture and the powders milled for different times. It can be found that the characteristic peaks of Al and α-Fe phases became weak with the increase of milling time. The initially sharp diffraction peaks of the fcc structure of Al significantly decreased, and in particular the (311) diffraction peak completely disappeared after ball milling for 24 h. In the same time, the Fe diffraction peaks exhibited a gradual broadening and a shifting toward lower diffraction angles, which can be clearly observed in a range of diffraction angles $2\theta = 42\text{-}47°$ as shown in Fig. 1b.

The broadening of Fe diffraction peaks indicated a grain size refinement and the introduction of internal strains. The shifting of Fe diffraction peaks toward a lower diffraction angle suggested an increase in the lattice parameter of Fe after milling and the formation of a bcc Fe-based solid solution, although a fraction of Al was still not dissolved into Fe under present milling condition. Moreover, the superlattice diffraction peaks of FeAl were not observed in those mechanical alloying processes, which further indicated that the final powder was supersaturated Fe(Al) solid solution. The broadening of the (110) peak of bcc-Fe was used to quantitatively estimate the grain size of the powder milled for different times through the Scherrer formula. After 36 h of milling, the average grain size was reduced to approximately 37 nm.

Figure 2 shows the typical microstructures of the cross sections of the Fe-Al powders milled for different times. The different element constituents showed different degrees of plastic deformation during ball milling. After 0.5 h milling, it was found that Fe particles have embedded in the continuous soft Al matrix and still kept their initial irregular morphology due to high-yield strength, as shown in Fig. 2a. With continuous milling to 2 h, Fe particles were clearly elongated because of intensive plastic deformation which resulted from collision against milling-balls and finally, a layered structure was formed due to cold welding, as shown in Fig. 2b and c. However, the single layer was still thick and about 10-20 μm in thickness. Further milling resulted in a refined lamellar structure, as shown in Fig. 2d. At a milling time of 10 h, the lamellar structure became more refined and uniform, as shown in Fig. 2e. Moreover, it was found that some cracks appeared in the interior of the powder (as shown by arrow), which was caused by the intense fracturing effect of the cold welding at this milling stage. The cracks will continuously grow with further milling, which results in fracture of larger particles into smaller ones. After milling for 24 h, the lamellar structure in the powder became more refined, as shown in Fig. 2f. Therefore, it can be seen that the microstructural evolution of Fe-40Al powder is a typical ductile-ductile mechanical alloying process via a layer-structure during ball milling (Ref 31).

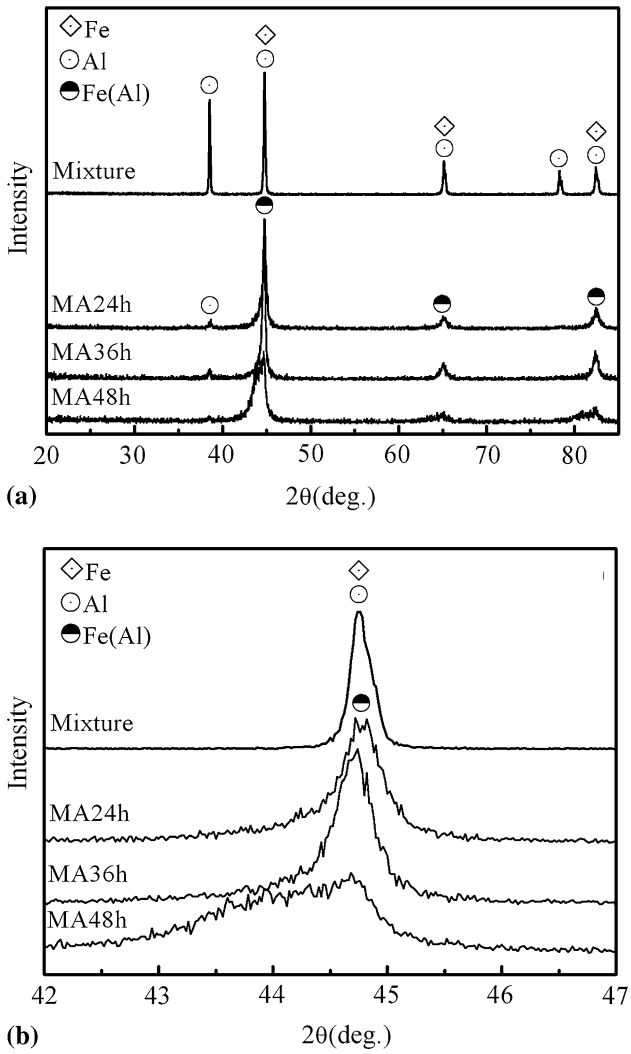


**Fig. 1** XRD patterns of the initial mixed powder and the powders ball-milled for different times (a). (b) is a zoom of main diffraction peak of Fe

To make a detailed examination into the microstructure and composition of the milled powder, SEM and EDXA were used to analyze the powder. Figure 3 shows typical SEM images of the morphologies and cross-sectional microstructures of the powder milled for 36 h

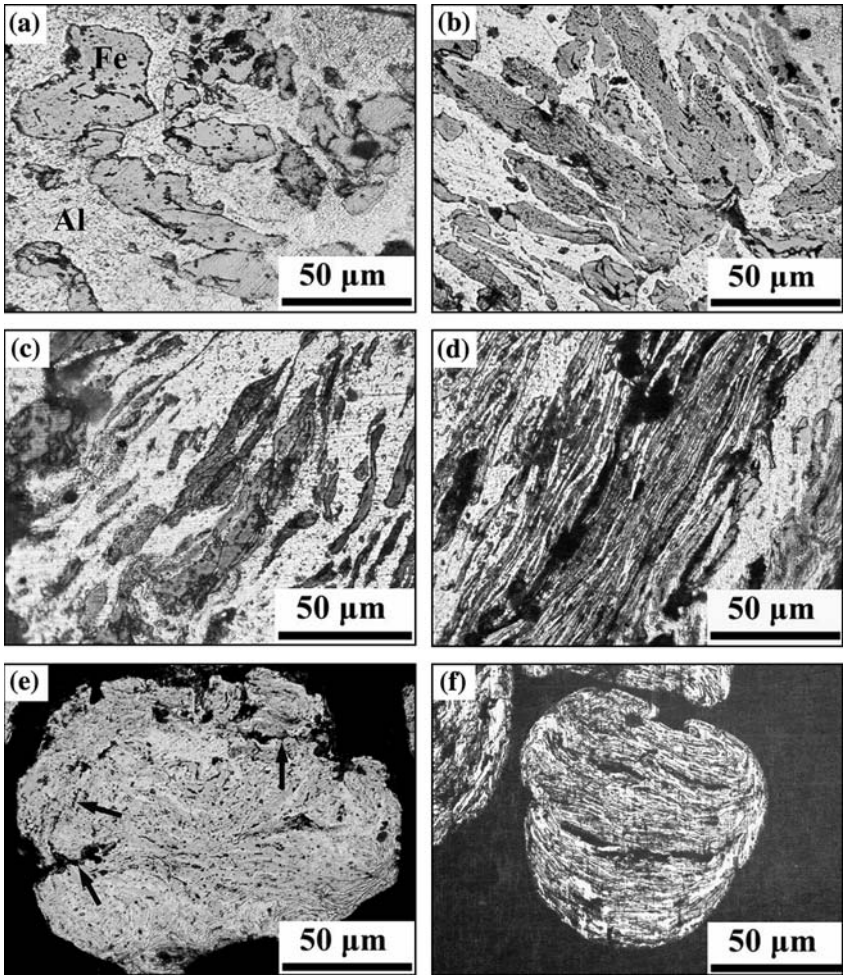


**Fig. 2** Typical cross-sectional optical microstructure of Fe-40Al powder after ball milling for different times: (a) 0.5 h, (b) 1 h, (c) 2 h, (d) 5 h, (e) 10 h, and (f) 24 h

(described as-milled powder hereafter), which was used as the feedstock powder to deposit coating. It can be seen that the as-milled powder presented in the aggregated condition showed an irregular angular morphology (Fig. 3a). The cross-sectional microstructure of the as-milled powder is shown in Fig. 3b. It can be seen that a fine lamellar structure was present in the powder. Meanwhile, a few relatively thicker layers were still present in the powder. This lamellar structure was also reported by Skoglund et al. (Ref 32). It was observed that these thicker layers will become thinner with further milling. The particle size distribution of as-milled powder is shown in Fig. 4, it can be seen that the distribution of particle size was homogenous with an average of approximately 20 μm, which was suitable for cold spraying.

Figure 5 shows a detailed microstructure of a cross section of the milled powder. Two distinguishable regions with different microstructural characteristics can be clearly seen. They were typically different in the lamellar thickness. EDXA analysis suggested that the thicker layer

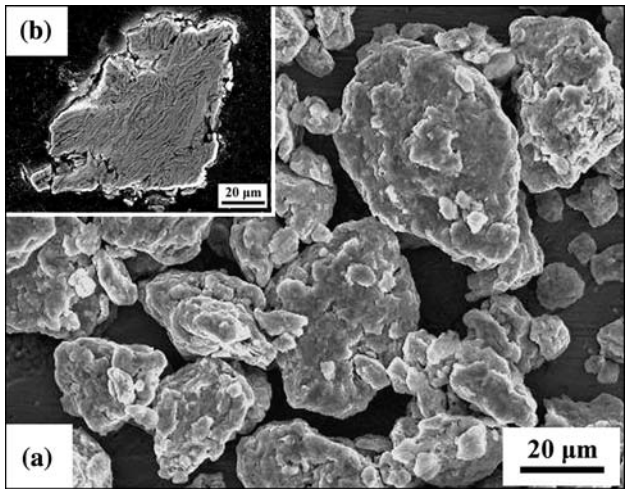


**Fig. 3** Morphology (a) and cross-sectional microstructure (b) of the as-milled powder

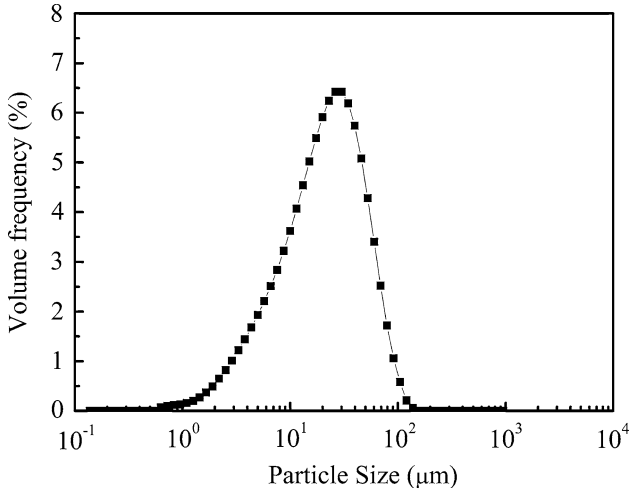


**Fig. 4** Particle-size distribution of as-milled Fe-40Al powder

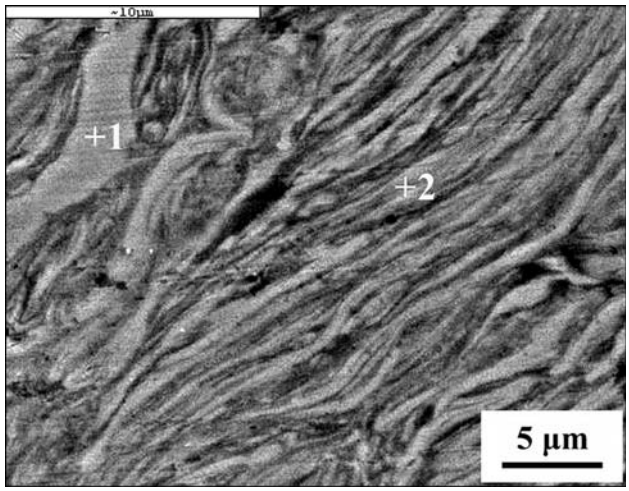


**Fig. 5** Typical lamellar microstructure of ball-milled Fe-Al alloy powder observed at a higher magnification shown in Fig. 3b

**Table 1 EDXA results of the points marked in Fig. 5**

| Positions | Al K (at.%) | Fe K (at.%) |
|---|---|---|
| Point 1 | 15.66 | 84.34 |
| Point 2 | 44.35 | 55.65 |

was a Fe-rich phase and the fine lamella was a Fe-Al solid solution with high-Al content, as indicated by the results shown in Table 1. In cold-spraying process, the particle deposition takes place in a solid state, and consequently, this lamellar structure of the milled powder will be completely transferred into the coating, giving a unique effect on the microstructure and properties of the cold-sprayed coating.

### 3.2 Characterization of the Cold-Sprayed Coatings

XRD patterns of the as-sprayed coating and feedstock powder are shown in Fig. 6. It was clear that the XRD

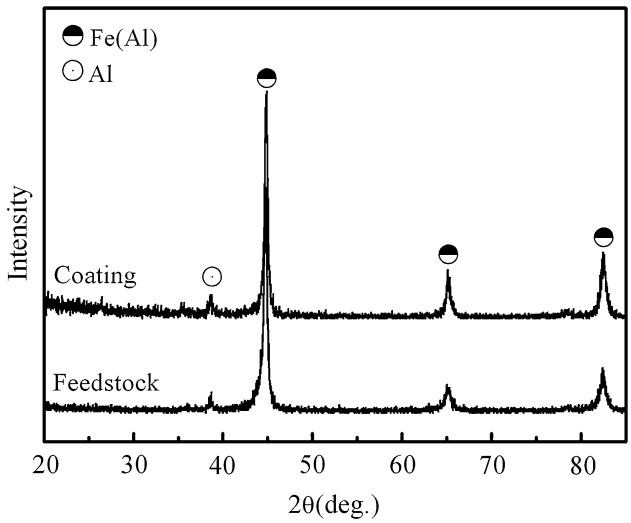


**Fig. 6** XRD patterns of the as-sprayed coating and the feedstock powder

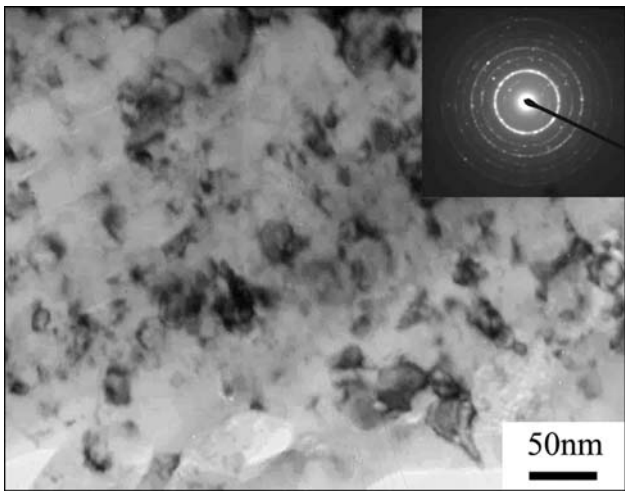


**Fig. 7** Bright-field TEM image of the as-sprayed Fe(Al) alloy coating

pattern of the coating was almost the same as that of the milled powder. This fact indicates that the coating and feedstock exhibited the same phase structure. The oxygen content of the as-sprayed coating was 1.8 wt.%, which was much lower than that of the coating (13-15 wt.%) deposited by HVOF spraying of the milled FeAl powder (Ref 33). No peaks corresponding to oxide phase were identified in the coating (as shown in Fig. 6), which was found in the coating deposited by HVOF of the milled FeAl powder (Ref 34). Wolski et al. (Ref 35) found that oxygen in the as-milled powder was present probably as uncrystallized oxides and no peaks corresponding to oxide phase were detected even though oxygen content in the milled FeAl powders was 9.5 wt.%. The average grain size of coating estimated by Scherrer formula was about 27 nm. A TEM bright-field image of the as-sprayed coating was

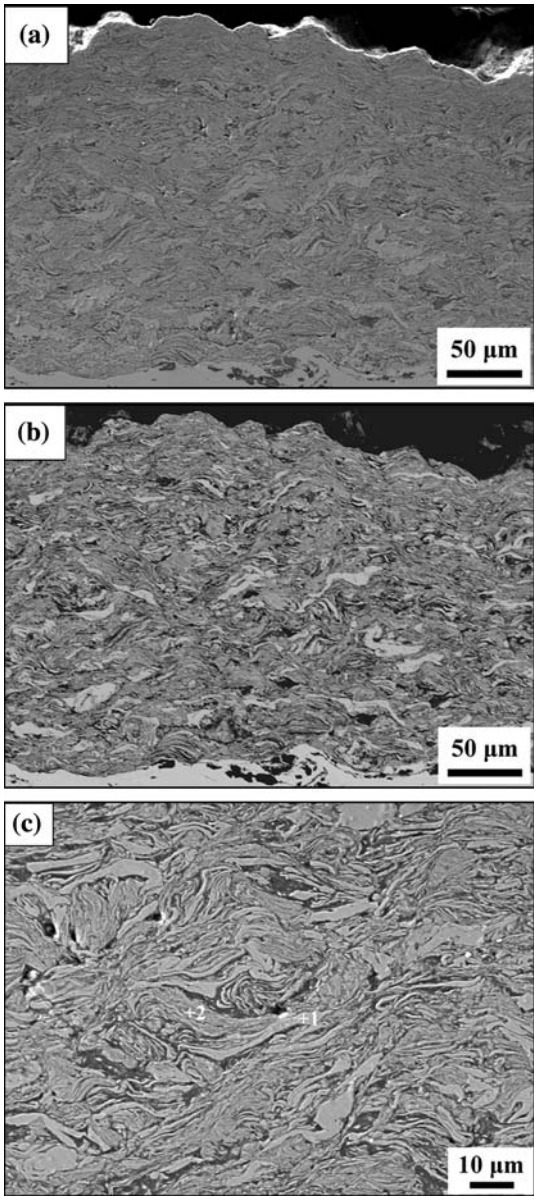


**Fig. 8** SEM images of the as-sprayed coating in (a) secondary electron mode, (b) back scattered electron mode, and (c) typical lamellar microstructure of as-sprayed coating observed at a higher magnification shown in Fig. 8a

shown in Fig. 7. The coating was clearly composed of grains of size ranging from 10 to 50 nm, which substantiated the average grain size (27 nm) estimated by XRD analysis. The corresponding SAD pattern shows whose radii agree with the bcc-α-Fe structure. It can be clearly recognized that the nanostructured Fe(Al) solid solution alloy coating was produced by cold spraying of the ball-milled Fe-40Al powder.

Figure 8 shows the typical microstructure of the as-sprayed coating. It was observed that the coating exhibited a very dense microstructure and some thicker layers with a white contrast appeared on the coating microstructure, which were clearly seen in back-scattered SEM image

**Table 2 EDXA results of the points marked in Fig. 8c**

| Positions | Al K (at.%) | Fe K (at.%) |
|---|---|---|
| Point 1 | 5.70 | 94.30 |
| Point 2 | 40.97 | 59.03 |

**Table 3 Chemical composition of as-milled powder and coating before and after heat treatment at 500 °C for 25 h (values in wt.%)**

| Material | Fe | Al | O | Cr | Ni |
|---|---|---|---|---|---|
| As-milled powder | 58.253 | 39.978 | 1.729 | 0.0237 | 0.0163 |
| As-sprayed coating | 58.025 | 40.123 | 1.812 | 0.0236 | 0.0164 |
| Heat-treated coating | 58.019 | 40.116 | 1.825 | 0.0236 | 0.0164 |

(Fig. 8b). According to EDXA analysis of the microstructure of the coating (Fig. 8c), the thicker layer was a Fe-rich phase and the fine lamella was a Fe-Al solid solution with high-Al content, as indicated by the results shown in Table 2. Moreover, from the Fig. 8c, it was noticeable that the lamellar microstructure of this coating was different from that of the cold-sprayed coating using the non-milled (metallic) powder mixture such as the blends of Ni/Al powders (Ref 36) and Ti/Al powders (Ref 37) because it evolved not only from the particle deformation, but also from the inner microstructure of the milled powder. Therefore, it was difficult to distinguish a single deformed particle and the particle boundary in the coating.

### 3.3 Effect of Heat treatment on the Evolution of the FeAl Intermetallic Compound Coating

FeAl intermetallic compounds exhibit excellent oxidation and corrosion resistance due to their ability to form a highly protective $Al_2O_3$ scale during exposure above 500 °C. However, the phase structure of the as-sprayed coating was just Fe-based solid solution. Therefore, the as-sprayed coatings need to be heat treated to obtain the expected FeAl intermetallic compound phase. Therefore, the as-sprayed coating was heat treated at temperatures from 200 to 500 °C for 25 h to examine the effect of heat treatment temperature on its phase structure. Chemical analysis of the as-milled powder and coating before and after heat treatment at temperatures 500 °C for 25 h are shown in Table 3. It can be seen that the content of O, Cr, and Ni between the as-milled powder and coating was almost same. The presence of Cr and Ni in the as-milled powder and coating was attributed to the stainless steel balls used as the milling media. Oxygen contamination can be attributed to a small volume of air entering the container during milling and to the transfer of the powder from the milling apparatus to an argon-protective container.

The XRD analysis results are shown in Fig. 9. It can be seen that the phase structure of the coating heat treated at a temperature of 200 °C was the same as that of the as-sprayed coating. After heat treatment at 300 °C, the phase transformation began and a trace of FeAl phase appeared

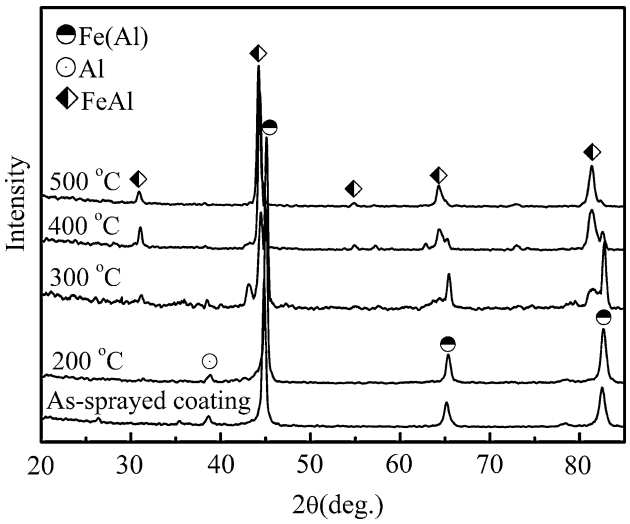


**Fig. 9** XRD patterns of as-sprayed and heat-treated coatings

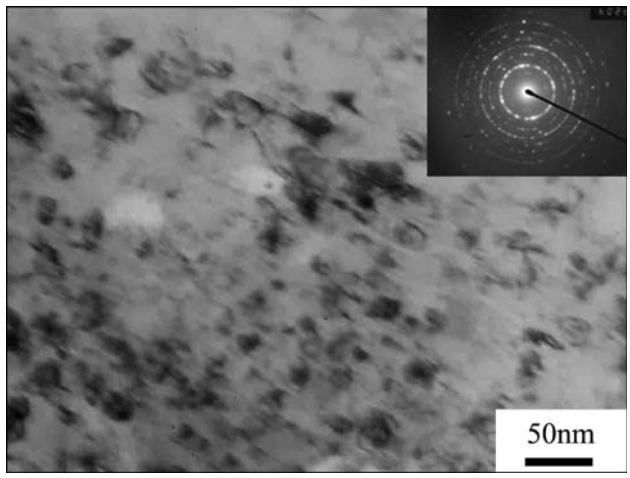


**Fig. 10** Bright-field TEM image of the nanostructured FeAl intermetallic coating after heat treatment at 500 °C for 25 h

in the coating. However, most of the phase was still Fe(Al) solid solution. This means that only a little part of Fe-Al alloy transformed to FeAl under this condition. With heat treatment temperature rising to 400 °C, the content of the FeAl phase in the coating was obviously increased, which can be seen from the intensity of FeAl diffraction peaks in the XRD patterns. Moreover, the superlattice diffraction peak of FeAl became obvious in XRD pattern. However, a fraction of Fe(Al) still was retained in the coating. When heat-treatment temperature was raised to 500 °C, the diffraction peaks of Fe disappeared completely and only diffraction peaks of FeAl intermetallic compound phase were present in the XRD patterns. This fact means that the heat treatment at a temperature of 500 °C was sufficient to completely convert the metastable Fe-based solid solution into the intermetallic compound. As a result, FeAl intermetallic compound can evolve through heat treatment of cold-sprayed metastable Fe-Al alloy.

A TEM bright-field image of the coating after heat treatment at a temperature of 500 °C for 25 h was shown in Fig. 10. The coating was clearly composed of nanograins of size ranging from 10 to 50 nm, the corresponding SAD pattern shows whose radii agree with the FeAl phase. It can be clearly recognized that a nanostructured FeAl intermetallic compound coating was prepared by cold praying of the ball-milled Fe-40Al alloy powder and post-heat treatment. For pure Fe and Al, the recrystalization will take place when they are heat treated at temperatures of 450 and 80 °C, respectively. However, the as-sprayed coating was disordered supersaturated Fe(Al) solid solution, Perez et al. (Ref 38, 39), Huang et al. (Ref 40), and Jiang et al. (Ref 41) reported that the addition of Al in to Fe during ball milling can significantly improves the thermal stability of as-milled nanocrystalline Fe-Al alloy. They thought that the mechanism was attributed to be a combination of Al solute drag (Ref 42), Zener pinning (Ref 43, 44) by aluminum-iron oxide and aluminum oxide phases at grain boundaries, and reduction of grain boundary energy by Al segregation and chemical ordering (Ref 45-47), therefore, the cold-sprayed FeAl coating after heat treatment at a temperature of 500 °C for 25 h still kept nanostructure.

## 4. Conclusions

A metastable Fe(Al) alloy powder with morphology and size distribution suitable for cold spraying was produced by ball milling. The prepared powder exhibited a lamellar microstructure. The lamellae were continually refined with increasing ball-milling time. It was found that the metastable microstructure of the milled Fe(Al) feedstocks can be completely retained into the coating using cold spraying. The heat-treatment temperature has significant influence on the in-situ evolution of the intermetallic compound through the cold-sprayed metastable Fe-Al alloy. The FeAl intermetallic phase was formed during the heat treatment of the as-sprayed coatings at a temperature of 500 °C. The results revealed that nanostructured FeAl intermetallic compound coatings can be prepared by cold spraying of the ball-milled Fe-40Al powder and post-heat treatment.

### Acknowledgments

The present work is supported by the Key Project of the Ministry of Education of China (No.106145) and R&D Project of Shaanxi Province (No. 2005KW-31).

### References

1. A. Papyrin, Cold Spray Technology, *Adv. Mater. Process.*, 2001, **159**(9), p 49-51
2. R.C. McCune, W.T. Donlon, O.O. Popoola, and E.L. Cartwright, Characterization of Copper Layers Produced by Cold Gas-Dynamic Spraying, *J. Therm. Spray Technol.*, 2000, **9**, p 73-82

3. H.K. Kang and S.B. Kang, Tungsten/Copper Composite Deposits Produced by a Cold Spray, *Scripta Mater.*, 2003, **49**, p 1169-1174
4. C.-J. Li and W.-Y. Li, Deposition Characteristics of Titanium Coating in Cold Spraying, *Surf. Coat. Technol.*, 2003, **167**, p 278-283
5. V. Shukla, G.S. Elliott, B.H. Kear, and L.E. McCandlish, Hyperkinetic Deposition of Nanopowder by Supersonic Rectangular Jet Impingement, *Scripta Mater.*, 2001, **44**, p 2179-2182
6. R.S. Lima, J. Karthikeyan, C.M. Kay, J. Lindemann, and C.C. Berndt, Microstructural Characteristics of Cold-Sprayed Nanostructured WC-Co Coatings, *Thin Solid Films*, 2002, **416**, p 129-135
7. C.-J. Li, W.-Y. Li, W.-H. Ma, and H. Fukanuma, Characterization of Microstructure of Nanostructured Fe-Si Coating Deposited by Cold Spraying, *Thermal Spray Solutions: Advances in Technology and Application*, DVS, Düsseldorf, 2004, p 371-377
8. L. Ajdelsztajn, B. Jodoin, G.E. Kim, and J.M. Schoenung, Cold Spray Deposition of Nanocrystalline Aluminum Alloys, *Met. Mat. Trans. A*, 2005, **36**, p 657-666
9. C.C. Koch, Synthesis of Nanostructured Materials by Mechanical Milling: Problems and Opportunities, *Nanostruct. Mater.*, 1997, **9**, p 13-22
10. P. Richer, B. Jodoin, E. Sansoucy, L. Ajdelsztajn, and G. E. Kim, Properties of Cold Spray Nickel Based Coatings, *ITSC 2006 Proceedings*, Seattle, USA, May 15-18, 2006
11. V.K. Sikka, J.T. Mavity, and K. Anderson, Processing of Nickel Aluminides and Their Industrial Applications, *Mater. Sci. Eng. A*, 1992, **153**, p 712-721
12. C.C. Koch, Intermetallic Matrix Composites Prepared by Mechanical Alloying—A Review, *Mater. Sci. Eng. A*, 1998, **244**, p 39-48
13. T.E. Mitchell, J.P. Hirth, and A. Misra, Apparent Activation Energy and Stress Exponent in Materials with A High Peierls Stress, *Acta Mater.*, 2002, **50**, p 1087-1093
14. N.S. Stoloff, Iron Aluminides: Present Status and Future Prospects, *Mater. Sci. Eng. A*, 1998, **258**, p 1-14
15. P.F. Tortorelli and K. Natesan, Critical Factors Affecting the High-Temperature Corrosion Performance of Iron Aluminides, *Mater. Sci. Eng. A*, 1998, **258**, p 115-125
16. Y. Yang and I. Baker, The Influence of Vacancy Concentration on the Mechanical Behavior of Fe-40Al, *Intermetallics*, 1998, **6**, p 167-175
17. I. Baker, X. Li, H. Xiao, R. Carleton, and E.P. George, The Room Temperature Strengthening Effect of Boron as a Function of Aluminum Concentration in FeAl, *Intermetallics*, 1998, **6**, p 177-183
18. M.A. Muñoz-Morris, C. Garcia Oca, and D.G. Morris, Microstructure and Room Temperature Strength of Fe-40Al Containing Nanocrystalline Oxide Particle, *Acta Mater.*, 2003, **51**, p 5187-5197
19. D.G. Morris and S. Gunther, Strength and Ductility of Fe-40Al Alloy Prepared by Mechanical Alloying, *Mater. Sci. Eng. A*, 1996, **208**, p 7-19
20. M.A. Morris-Muñoz, A. Dodge, and D.G. Morris, Structure, Strength and Toughness of Nanocrystalline FeAl, *Nanostruct. Mater.*, 1999, **11**, p 873-885
21. M. Hoffmann and R. Birringer, Elastic and Plastic Behavior of Submicrometer-sized Polycrystalline NiAl, *Acta Mater.*, 1996, **44**, p 2729-2736
22. M. Krasnowski and T. Kulik, Nanocrystalline FeAl Intermetallic Produced by Mechanical Alloying Followed by Hot-Pressing Consolidation, *Intermetallics*, 2007, **15**, p 201-205
23. M.A. Morrisand and M. Leboeuf, Grain-size Refinement of γ-Ti-Al Alloys: Effect on Mechanical Properties, *Mater. Sci. Eng. A*, 1997, **224**, p 1-11
24. T.R. Malow and C.C. Koch, Mechanical Properties in Tension of Mechanically Attrited Nanocrystalline Iron by the Use of the Miniaturized Disk Bend Test, *Acta Mater.*, 1998, **46**, p 6459-6473
25. H.G. Jiang, M.L. Lau, and E.J. Lavernia, Grain Growth Behavior of Nanocrystalline Inconel 718 and Ni Powders and Coatings, *Nanostruct. Mater.*, 1998, **10**, p 169-178
26. J.A. Hearley, J.A. Little, and A.J. Sturgeon, The Effect of Spray Parameters on the Properties of High Velocity Oxy-Fuel NiAl Intermetallic Coatings, *Surf. Coat. Technol.*, 2000, **123**, p 210-218
27. T. Grosdidier, A. Tidu, and H.L. Liao, Nanocrystalline Fe-40Al Coating Prepared by Thermal Spraying of Milled Powder, *Scipta Mater.*, 2001, **44**, p 387-393
28. H.-T. Wang, C.-J. Li, G.-J. Yang, and C.-X. Li, Formation of Fe-Al Intermetallic Compound Coating Through Cold Spraying, *ITSC 2006 Proceedings*, Seattle, USA, May 15-18, 2006
29. B.D. Cullity and S.R. Stock, Elements of X-ray Diffraction, (3rd ed.). Prentice Hall, Upper Saddle River, NJ, 2001, p 399-402
30. L. Shaw, H. Luo, J. Villegas, and D. Miracle, Thermal Stability of Nanostructured Al93Fe3Cr2Ti2 Alloys Prepared via Mechanical Alloying, *Acta. Meter.*, 2003, **51**, p 2647-2663
31. C. Suryanarayana, Mechanical Alloying and Milling, *Prog. Mater. Sci.*, 2001, **46**, p 1-184
32. H. Skoglund, M.K. Wedel, and B. Karlsson, The Role of Oxygen in Powder Processing of FeAl, *Intermetallics*, 2003, **11**, p 475-482
33. G. Ji, O. Elkedim, and T. Grosdidier, Deposition and Corrosion Resistance of HVOF Sprayed Nanocrystalline Iron Aluminide Coatings, *Surf. Coat. Technol.*, 2005, **190**, p 406-416
34. M. Fukumoto, W, Hu, T. Katoh, and M. Yamasaki, Synthesis of Nanocrystalline Iron Aluminide Intermetallic Compound Coating by Spraying of Mechanically Alloyed Powder, *ITSC 2004 Proceedings*, Osaka, Japan, May 10-12, 2004
35. K. Wolski, F. Thévenot, and J. le Coze, Effect of Nanometric Oxide Dispersion on Creep Resistance of ODS-FeAl Prepared by Mechanical Alloying, *Intermetallics*, 1996, **4**, p 299-307
36. H.Y. Lee, S.H. Jung, S.Y. Lee, and K.H. Ko, Alloying of Cold-sprayed Al-Ni Composite Coatings by Post-annealing, *Appl. Surf. Sci.*, 2007, **253**, p 3496-3502
37. T. Novoselova, S. Celotto, R. Morgan, P. Fox, and W. O'Neill, Formation of TiAl Intermetallics by Heat Treatment of Cold-Sprayed Precursor Deposits, *J. Alloys Compd.*, 2007, **436**, p 69-77
38. R.J. Perez, B. Huang, and E.J. Lavernia, Thermal Stability of Nanocrystalline Fe-10 wt.% Al Produced by Cryogenic Mechanical Alloying, *Nanostruct. Mater.*, 1996, **7**, p 565-572
39. R.J. Perez, H.G. Jiang, and E.J. Lavernia, Grain Size Stability of Nanocrystalline Cryomilled Fe-3 wt.% Al alloy, *Nanostruct. Mater.*, 1997, **9**, p 71-74
40. B. Huang, R.J. Perez, and E.J. Lavernia, Grain Growth of Nanocrystalline Fe-Al Alloys Produced by Cryomilling in Liquid Argon and Nitrogen, *Mater. Sci. Eng. A*, 1998, **255**, p 124-132
41. H.G. Jiang, H.M. Hu, and E.J. Lavernia, Synthesis of Fe-rich Fe-Al Nanocrystalline Solid Solutions Using Ball Milling, *J. Mater. Res.*, 1999, **14**, p 1760-1770
42. P. Knauth, A. Charaï, and P. Gas, Grain Growth of Pure Nickel and of a Ni-Si Solid Solution Studied by Differential Scanning Calorimetry on Nanometer-Sized Crystals, *Scripta Metall. Mater.*, 1993, **28**, p 325-330
43. H.J. Höfler and R.S. Averback, Grain Growth in Nanocrystalline $TiO_2$ and Its Relation to Vickers Hardness and Fracture Toughness, *Scripta Metall. Mater.*, 1990, **24**, p 2401-2406
44. K. Boylan, D. Ostrander, U. Erb, G. Palumbo, and K.T. Aust, An In-Situ Tem Study of the Thermal Stability of Nanocrystalline Ni_P, *Scripta Metall. Mater.*, 1991, **25**, p 2711-2716
45. Z. Gao and B. Fultz, The Thermal Stability of Nonocrystalline Fe-Si-Nb Prepared by Mechanical Alloying, *Nanostruct. Mater.*, 1993, **2**, p 231-240
46. Z. Gao and B. Fultz, Inter-Dependence of Grain Growth, Nb Segregation, and Chemical Ordering in Fe-Si-Nb Nanocrystals, *Nanostruct. Mater.*, 1994, **4**, p 939-947
47. C. Bansal, Z.Q. Gao, and B. Fultz, Grain Growth and Chemical Ordering in $(Fe, Mn)_3Si$, *Nanostruct. Mater.*, 1995, **5**, p 327-336